CHEMISTRY
A European Journal

A Journal of
ChemPubSoc Europe

Accepted Article

Title: Intrinsic and Extrinsic Heavy Atom Effect on the Multifaceted Emissive Behavior of Cyclic Triimidazole

Authors: Elena Maria Cariati, Elena Lucenti, Alessandra Forni, Chiara Botta, Clelia Giannini, Daniele Malpicci, Daniele Marinotto, Andrea Previtali, and Stefania Righetto

To be cited as: *Chem. Eur. J.* 10.1002/chem.201804980

Link to VoR: http://dx.doi.org/10.1002/chem.201804980

Supported by
ACES

WILEY-VCH

10.1002/chem.201804980

COMMUNICATION

WILEY-VCH

Intrinsic and Extrinsic Heavy Atom Effect on the Multifaceted Emissive Behavior of Cyclic Triimidazole

Elena Lucenti,[a] Alessandra Forni,*[a] Chiara Botta,*[b] Clelia Giannini,[c] Daniele Malpicci,[c] Daniele Marinotto,[a] Andrea Previtali,[c] Stefania Righetto[c] and Elena Cariati*[c]

Abstract: Since heavy halogen atoms can be used to tune the emissive properties of organic luminogens, the understanding of their role in the photophysics is fundamental for materials engineering. Here, the extrinsic and intrinsic heavy atom effects on the photophysics of organic crystals are separately evaluated by comparing cyclic triimidazole (**TT**) with its mono-iodo derivative (**TTI**) and its cocrystal with diiodotetrafluorobenzene (**TTCo**). Crystals of **TT** show room temperature ultralong phosphorescence (RTUP) originated from H-aggregation. **TTI** and **TTCo** display two additional long lived components whose origin is elucidated through single crystal X-ray and DFT-TDDFT studies. The results highlight the different effects of the I atom on the three phosphorescent emissions. Intrinsic heavy atom effects play a major role on molecular phosphorescence which is displayed at RT only for **TTI**. H-aggregate RTUP and the I···N XB induced phosphorescences on the other side depend only on packing features.

Room temperature phosphorescence (RTP) from solid-state purely organic materials[1] represents a relatively new issue in the development of functional materials for phosphor applications, despite the growing demand in this field. With respect to their organometallic counterparts, they offer many advantages such as lower toxicity, cost and environmental load. Moreover, specific features potentially associated with organic phosphorescent materials, such as long afterglow lifetimes, have opened the way to new possible applications including low-cost data security technologies,[2] temperature monitoring, sensing and bio-imaging.[1c,2]

The possibility to switch on RTP and/or modulate phosphorescence properties (e.g., efficiency, lifetimes and excitation/emission energy) of organic luminophors in solid state through specific intra- and intermolecular interactions represents a valuable tool in view of functional applications.[3] In particular, the heavy atom effect can be tuned, for example, by either introducing into the molecules (intrinsic effect) a halogen atom (Br or I)[4] or by exploiting specific intermolecular interactions (extrinsic effect) based on halogen bonding with other molecules of the same type (one component)[5] or a different type (two-component) such as for example in co-crystals.[6] According to the different XB (halogen bond) pattern, various effects can be produced either in fluorescence or phosphorescence. In this regard, we have recently reported the photophysical behavior of two triimidazo[1,2-a:1',2'-c:1'',2''-e][1,3,5]triazine (**TT**) derivatives, namely 3,7-dibromotriimidazo[1,2-a:1',2'-c:1'',2''-e][1,3,5]triazine, **2Br** and 3,7,11-tribromotriimidazo[1,2-a:1',2'-c:1'',2''-e][1,3,5]triazine, **3Br** (Scheme 1), in which such an extrinsic single component effect, combined with the intrinsic one, is clearly demonstrated.[7] In fact, **2Br** whose structure displays strong and rigid Br_4 XB intermolecular unit, shows an induced long lived RTP which is absent in **3Br** having a looser not planar Br_3 XB unit.

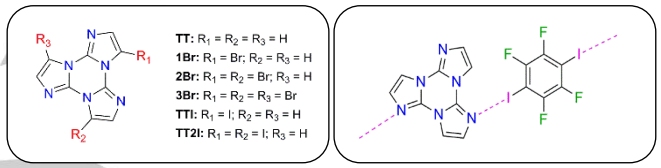

Scheme 1. Chemical structures of **TT** and its halogenated derivatives (left panel), and of **TTCo** (right panel).

Here, in view of deepening the knowledge of the extrinsic/intrinsic effects, we investigate the structural and emissive properties of 3-iodiotriimidazo[1,2-*a*:1',2'-*c*:1'',2''-*e*][1,3,5]triazine, **TTI**, and **TTCo**, the 1:1 cocrystal self-assembled through I···N XB between two acceptor nitrogen atoms of **TT** and the two iodine atoms of 1,4-diiodotetrafluorobenzene, **DITFB**, to form a 1D infinite chain structure (see Scheme 1). **TTI** is the prototype of intrinsic halogen atom effects and its comparative study with the bromine **TT** analogues allows to evaluate the role played by I vs. Br. This investigation is further deepened by preliminary photophysical and structural analysis of **TT2I** (3,7-diiodotriimidazo[1,2-*a*:1',2'-c:1'',2''-*e*][1,3,5]triazine). On the other side, **TTCo**, where I···N XB guarantees a strong non-covalent interaction between iodine atom and the luminophor, allows to isolate the extrinsic two-component effect by comparison with the **TTI** and **TT** photoluminescent properties. The latter is characterized by crystallization induced and mechanochromic emissive behavior, together with room temperature ultralong phosphorescence (RTUP) at ambient conditions (lifetime up to 1s, see Table S1) associated with H-aggregation which provides the necessary stabilization of the triplet excitons.[8]

Solutions of **TTI** in DCM (10^{-4}M) display an absorption band at about 240 nm and no emission at RT. At 77K a hardly discernible emission at about 420 nm appears by exciting at low energy (λ_{exc}=340nm) and an intense, broad phosphorescence at about 630 nm (τ_{av}=27.27μs) dominates the spectrum by exciting at high energy (below 300nm; see Figure 1a and Table S1). The behavior of **TTI** in solution is similar to that of **1Br**, **2Br** and **3Br**,

[a] Dr. E. Lucenti, Dr. A. Forni, Dr. D. Marinotto
ISTM-CNR, INSTM RU
via Golgi 19, 20133 Milano, Italy.
E-mail: alessandra.forni@istm.cnr.it
[b] Dr. C. Botta
ISMAC-CNR, INSTM RU
Via Corti 12, 20133 Milano, Italy.
E-mail: chiara.botta@ismac.cnr.it
[c] Dr. C. Giannini, Dr. D. Malpicci, Dr. A. Previtali, Dr. S. Righetto, Prof. E. Cariati
Dept. of Chemistry, Università degli Studi di Milano and INSTM RU
via Golgi 19, 20133 Milano, Italy.
E-mail: elena.cariati@unimi.it

Supporting information for this article is given via a link at the end of the document.

10.1002/chem.201804980

even though some differences are noteworthy, i.e.: (i) while for Br derivatives the weak fluorescence, observed also at 298K (at 328 nm for **1Br**), was ascribed to emission from higher singlet level, in the case of **TTI** it appears as a weak band only at 77 K with an energy position compatible with deactivation from the S_1 level; (ii) the molecular phosphorescence (MP) of **TTI** is largely red-shifted (by about 50 nm) with respect to that of the Br derivatives (575-585 nm); (iii) the lifetime of the MP is one order of magnitude shorter than those of **1Br**, **2Br** and **3Br** (τ_{av}=263-288μs); and (iv) the PLQY (Φ) is almost 0%, as observed for **2Br** and **3Br**, while is 3% for **1Br**. Observations (iii) and (iv) are in agreement with the enhanced heavy atom effect of iodine with respect to bromine, magnifying the Spin-Orbit Coupling (SOC) so as to make both singlet-to-triplet and triplet-to-singlet ISCs more efficient. These processes, in that order, decrease fluorescence and speed up the MP. As in the case of the bromine derivatives, the MP is explained by the presence, in the computed TDDFT excitation energies (see Figures S42, S43 and Tables S3, S4), of a $^3(\sigma,\sigma^*)$ state (T_5) close to a singlet state of $^1(\pi,\pi^*)$ character allowing SOC. Moreover, a direct comparison with the excitation energies of **1Br** (see Figure S42) shows that the $^3(\sigma,\sigma^*)$ state is located at much lower energy justifying the observed red-shift of the emission.

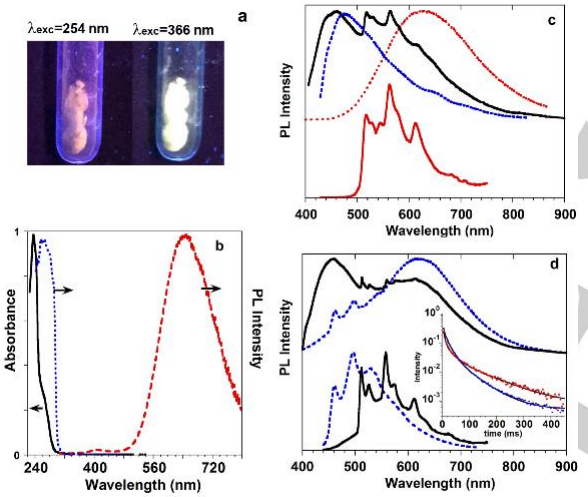

Figure 1. a) Pictures of **TTI** crystals under UV illumination at 298K; b) **TTI** in DCM: absorption spectrum at 298K (black solid line); emission and excitation spectra at 77K (λ_{exc}=280nm, red dashed line; λ_{em}=648nm, blue dotted line); c) emission spectra of **TTI** crystals at 298K: Top: PL at λ_{exc}=300nm (red dotted line), λ_{exc}=370nm (black solid line), λ_{exc}=415nm (blue dashed line); Bottom: Phosphorescence spectrum (λ_{exc}=370nm, delay 50ms, window 200ms, red solid line,); d) Emission spectra of **TTI** crystals at 77K. Top: PL at λ_{exc}=320nm (blue dotted line), λ_{exc}=370nm (black solid line); Bottom: Phosphorescence spectra at λ_{exc}=320nm (delay 10ms, window 50ms, blue dotted line) and λ_{exc}=370nm (delay 50ms, window 200ms, black solid line). Phosphorescence decays at λ_{em}=460nm (λ_{exc}=320nm, blue points) and λ_{em}=558nm (λ_{exc}=370nm, red points) with their three-exponential fits (black lines) are shown in the inset.

The emissive properties of crystals of **TTI** at 298K (Φ <0.1%) are reported in Figure 1c and Table S1. By exciting at low energy (415 nm) a broad fluorescence at 476 nm (τ_{av}=1.37 ns) is observed. Contrarily to powders of **1Br** and **3Br**, which show dual fluorescence associated with emission from S_m and S_1 levels and **2Br** which emits only from S_m, **TTI** fluorescence originates from S_1 only, in agreement with what observed in solution. At slightly higher excitation energy (370nm), the fluorescent emission is superimposed to a structured ultralong phosphorescence (τ_{av}=63.69ms) at 517, 563, 612 nm well resolved in the delayed spectrum. By exciting at even shorter wavelengths (<300 nm) the low energy MP at about 630 nm is observed (τ_{av}= 0.53 μs). At 77K (Figure 1d and Table S1), an even more complex behavior is observed. By exciting at 370 nm a multicomponent emission appears in the spectrum as the result of the superimposition of the broad fluorescence at 458 nm (τ_{av}= 2.77 ns), the sharp peaks of the ultralong phosphorescence and the unresolved MP. The fluorescent emission together with the ultralong phosphorescence disappear by exciting at 320nm. At this energy the MP is superimposed to a new phosphorescence with peaks at 460 and 495nm. The two phosphorescence spectra, shown in the bottom of Figure 1d together with their decays, are separated by integration of the phosphorescence at different delays (λ_{exc}=370nm, 511,526-558,573-610 nm, τ_{av}= 66.47ms; λ_{exc}=320 nm, 460-495-530nm, τ_{av}= 34.85ms). Upon excitation at short wavelengths (λ_{exc}=280 nm) the strong MP at 640nm (τ=23.66μs) dominates the spectrum (Figure S15).

Single crystal X-ray diffraction studies reveal an intriguing and new self-assembled motif of **TTI** governed by XB and π-π stacking. The compound crystallizes in the *C*2/*c* space group with two independent molecules in the asymmetric unit (see Figures 2 and S35-37). The crystal structure is dominated by the formation of helicoidal chains along the *b* direction through non-equivalent I···N XB on either sides of the **TTI** molecules, a stronger one ($r_{I2\cdots N5}$ = 2.878 Å, corresponding to a shortening by 18% with respect to the sum of vdW radii) connecting essentially coplanar molecules, and a weaker one ($r_{N11\cdots I2}$ = 3.020 Å, shortening by 14%) connecting strongly twisted molecules (the dihedral angles between the l.s. planes through the triazinic rings of the interacting pair are 14.6 and 69.2°, respectively). Four molecules are present within the pitch, which is 16.388 Å long, and four chains are intervolved along the helix axis, so allowing rather short interplanar distances (3.309 Å) among luminophors. The reduced slippage (2.3 Å) of adjacent **TTI** molecules along the helix axis together with the distance between centroids of triazinic rings (4.097 Å) and the angle θ between the centroid-centroid vector and the projection of this vector on the molecular plane (55°) are indicative of H-aggregation, comparable to that found in **2Br**. The quadruple helices are laterally connected through relatively strong C–H···N ($r_{N7\cdots H17}$ = 2.38 Å and $r_{N1\cdots H16}$ = 2.50 Å) and weak C–H···I hydrogen bonds.

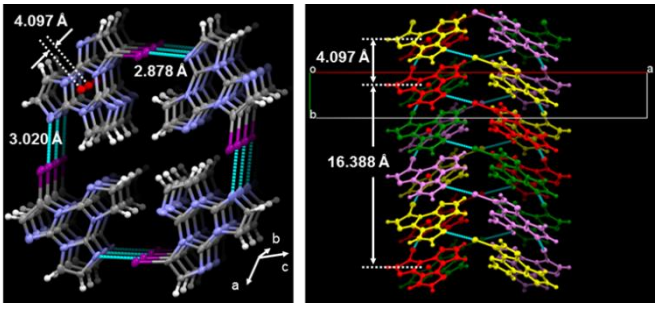

Figure 2. Partial views along *b*- (left) and *c*-axis (right) of **TTI** crystal structure showing columnar H-aggregates (centroids of the triazinic rings shown as red circles) interconnected through I···N XB (light blue dashed lines) to form intervolved quadruple helices along the *b*-axis.

10.1002/chem.201804980

In order to collect a better picture of the intrinsic effect of Iodine, we have synthetized and characterized **TT2I**. Its crystal structure is isomorphous with that of **2Br** consisting of slightly corrugated planes with molecules forming tetrameric I···I XB cyclic units that stack along the a axis with a rather small lateral shift (Figures S38, S39). The distance between the centroids of the triazine rings (4.304 Å) is longer than that of **2Br** (4.068 Å). Preliminary measurements on crystals of **TT2I** at 298K (see Figures S23-S26), reveal a photophysical behavior (Φ = 7%) similar to that of **TTI** with wavelength dependent emission spectra from which a fluorescence (443 nm, τ_{av}= 1.23 ns), a RTUP (625 nm, τ_{av}= 9.47ms) and a MP (680nm, τ_{av}= 3.47 ms) can be recognized.

In view of these observations, together with a comparison with the results previously obtained on the parent **TT** and its Br derivatives, we can draw the following conclusions: (i) the ultralong RTP of **TTI** and **TT2I** is ascribed to H-aggregation in their crystal structure in agreement with what reported for **TT**, **2Br** and **3Br**; (ii) the RTUP vibrational fine structure of **TTI**, better resolved than that of **TT**, **2Br** and **3Br**, could be justified by the stronger intermolecular I···N XB in the crystal structure of **TTI**, with respect to the weaker Br···N and Br···Br XBs in **2Br** and **3Br** and the even weaker C–H···N HB in **TT**; (iii) lifetimes τ_{av} of the RTUP, on the other hand, decrease in the order: **TT** (970ms) >> **TTI** (64 ms) > **2Br** (29ms) > **3Br** (18ms) > **TT2I** (9ms), as a consequence of the strength of H-aggregates (decreasing in the order **TT** > **TTI** ≃ **2Br** > **3Br** > **TT2I**) and the presence of heavy atoms; (iv) similar to **2Br** and **3Br**, the 77K phosphorescence of ms order observed at 460 nm is due to XB formation. Differently from **2Br** and **3Br**, where it was associated with homonuclear Br···Br XB (tetrameric and trimeric triimidazolic units in **2Br** and **3Br**, respectively, the former generating phosphorescent emission also at 298K), in **TTI** such phosphorescence is due to I···N heteronuclear XB. Interestingly, the analogous but weaker Br···N interaction present in **1Br** ($r_{Br\cdots N}$ = 3.006 Å, 12% shorter than the sum of vdW radii) does not give rise to similar phosphorescent emission; (v) for **TTI** and **TT2I** the MP is much more intense than that observed for all Br derivatives, so as to be clearly visible also at 298K in agreement with the presence of the heavier iodine atom on the molecule. Moreover, besides being usually activated by exciting at high energy, in the case of **TTI** the MP can be detected also by exciting S_1, though this is not verified in solution probably owing to the low oscillator strength of this state (see Figure S31).

The emissive properties of crystals of **TTCo** at 298K (Φ = 5%) are reported in Figure 3c and Table S1. A broad fluorescence with maximum at about 410 nm (τ_{av}=2.56 ns) and phosphorescence bands at 496, 528 and 566 nm (τ_{av}=21.48 ms) are observed by exciting at short wavelength (λ_{exc} ≤340 nm,). By exciting at longer wavelengths (λ_{exc} ≥340 nm) the vibronic components at low energy, the only visible in the delayed spectrum, are intensified. At 77K (Figure 3e and Table S1) a broad, red phosphorescence at 720nm (τ = 6.83 μs), dominates the spectrum by exciting at 300 nm or shorter wavelengths. Based on comparison with **TTI**, and confirmed by DFT/TDDFT calculations on the optimized dimeric model **TT·DITFB**, such emission is ascribed to the presence of iodine atom of the co-crystallized **DITFB** through extrinsic heavy atom effect. In fact, as in the cases of **TTI** and **TTBr**, the halogen atom generates $^3(\sigma,\sigma^*)$ and $^3(\pi,\sigma^*)$ levels allowing SOC from close singlet states of different character (Figure S42). In agreement with its lower efficiency with respect to the intrinsic effect observed in **TTI**, such 'extrinsic-MP', absent in **TT** crystals, is observed only at low temperature. By exciting at λ_{exc} ≥ 320nm a multicomponent emission comprising a fluorescence at 440 nm (τ_{av}= 3.41 ns), and two different phosphorescence components well resolved in the delayed spectra (see bottom of Figure 3e), one at 490, 527, 560 nm (τ_{av}=20.01ms) and the other at 463, 497, 537 nm (τ_{av}=14.65 ms), are observed.

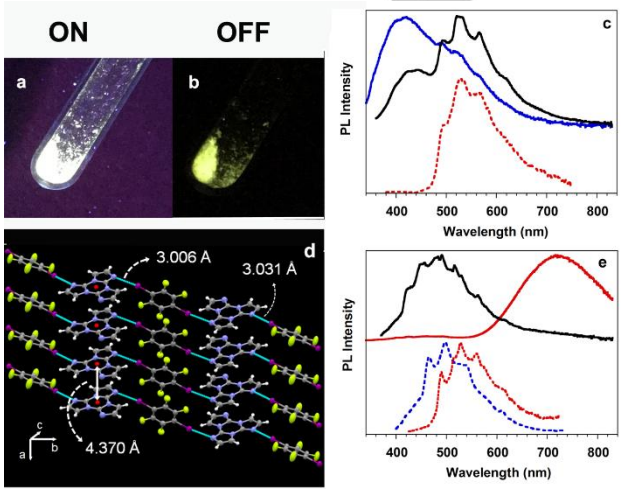

Figure 3. a,b) Images of **TTCo** crystals at 298K with UV illumination on and off; c) Emission spectra of **TTCo** at 298K: Top: PL at λ_{exc}=300nm (blue line) and λ_{exc}=350nm (black solid line); Bottom: Phosphorescence spectrum (λ_{exc}=350nm, delay 0.5ms, window 1ms, red dashed line); d) Partial view of the crystal structure of **TTCo** showing columnar H-aggregates of **TT** along the *a* direction (centroids of the triazinic rings shown as red circles) interconnected through I···N XB (light blue dashed) with **DITFB** to form infinite 1D zig-zag chains; e) Emission spectra of **TTCo** crystals at 77K: Top: PL at λ_{exc}=340nm (black line), λ_{exc}=300nm (red solid line); Bottom: Phosphorescence spectra at λ_{exc}=320nm (delay 10ms, window 50ms, blue dashed line) and λ_{exc}=370nm (delay 10ms, window 50ms, red dotted line).

Single crystal X-ray diffraction studies on **TTCo** show that the compound crystallizes in the $P2_1/n$ space group with one molecule of **TT** and two half molecules of **DITFB** in the asymmetric unit (Figures 3d and S40). The crystal structure consists of heteromeric zig-zag 1D chains self-assembled through I···N XB where **TT** acts as double XB acceptor and **DITFB** as double XB donor. The 1D chains are laterally connected through weak C–H···N and C–H···F hydrogen bonds. Along the chain the I···N distances, $r_{I1\cdots N1}$ = 3.031 Å (XB_1) and $r_{I2\cdots N5}$ = 3.006 Å (XB_2), are shorter by 14 and 15%, respectively, than the sum of their vdW radii. The interacting modules are far from coplanarity, as denoted by the dihedral angles between the l.s. planes through the triazinic ring and the **DITFB** unit, which are 31.51° (XB_1) and 77.36° (XB_2). Adjacent chains along the *a* direction are connected through strong π-π stacking interactions among **TT**s which are segregated from the two **DITFB** modules, each of them forming infinite columns with interplanar distances equal to 3.332, 3.488 and 3.777 Å, respectively. Compared with the **TTI** structure, the larger slippage (2.8 Å) and distance between centroids of **TT** triazinic rings (4.370 Å) along the column axis, together with the lower value of θ angle (50°) are indicative of weaker H-aggregates in **TTCo** with respect to **TTI**. In view of these structural features, the two rather overlapped phosphorescences of **TTCo** can be interpreted as follow. The longer lived one, visible also at room temperature, is associated with the presence of H aggregation of **TT** units, while the shorter one, visible only at low temperature, is originated from I···N XB.

Besides the already evidenced differences on the intrinsic effect exerted by the iodine atom with respect to the bromine one, the comparison between **TTI** and **TTCo** allows to drawn some conclusions. The presence of the iodine atom on the **TT** scaffold activates two additional phosphorescent deactivation channels. In fact, for both solids three 'critical' triplet state excitation wavelengths can be recognized (Figure 5): a 370 nm one which is responsible for the RTUP ($T_1^H \rightarrow S_0$); a 320 nm excitation which activates the low temperature I···N XB induced phosphorescence ($T_1^I \rightarrow S_0$) at similar position for **TTI** and **TTCo**, according to their common origin; a high energy (≤300nm) excitation which promotes the extrinsic or the intrinsic 'MP'($T_1 \rightarrow S_0$). Moreover, the extrinsic/intrinsic heavy atom effect manifests in the following aspects: i) the PLQY decreases from 5 to <0.1% going from **TTCo** to **TTI** but increases to 7% for **TT2I** (an increase in the PL QY was also observed on moving from **1Br** to **2Br**), suggesting that the rigidity of the crystal structure plays a major role in this regard; ii) room temperature 'MP' is observed only in **TTI** and **TT2I**, in agreement with a stronger intrinsic heavy atom effect; iii) at low temperature the 'extrinsic-MP' of **TTCo** is shifted in the NIR and is faster than that of **TTI**. A possible explanation of both experimental observations lies in the $^3(\sigma,\sigma^*)$ character of the emissive triplet having greater distortion in **TTCo** (due to the non bonded interaction); iv) the I···N XB induced phosphorescence is dependent on the strength of such interaction regardless its one- or two-component origin, being observed in both **TTI** and **TTCo**; v) The average lifetimes of $T_1^I \rightarrow S_0$ and $T_1^H \rightarrow S_0$ are longer for **TTI** in agreement with its stronger XB and H aggregate motives. In summary, our results demonstrate the effective role of intrinsic vs extrinsic heavy atom effect in tuning the phosphorescence properties of solid-state luminophors, offering an avenue to design efficient emissive materials for sensors, data security and bioimaging applications.

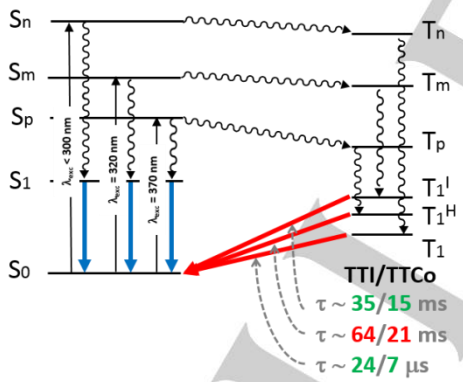

Figure 5. Energy level diagrams showing transitions associated with fluorescence (blue) and phosphorescence (red) with correspondent average lifetime (red, 298K and green, 77K) for crystals of **TTI** and **TTCo**. $T_1^I \rightarrow S_0$ is observed only at 77K, $T_1^H \rightarrow S_0$ is observed both at 298 and 77K, $T_1 \rightarrow S_0$ is observed at both 298 and 77K for **TTI** while only at 77K for **TTCo**.

Acknowledgements

The use of instrumentation purchased through the Regione Lombardia−Fondazione Cariplo joint SmartMatLab Project is gratefully acknowledged.

Keywords: co-crystal • halogen bonding • photophysics • room temperature phosphorescence • time resolved spectroscopy

[1] a) M. Baroncini, G. Bergamini, P. Ceroni, *Chem. Commun.* **2017**, *53*, 2081-2093; b) A. Forni, E. Lucenti, C. Botta, E. Cariati, *J. Mater. Chem. C* **2018**, *6*, 4603-4626; c) S. Hirata, *Adv. Opt. Mater.* **2017**, *5*, 1700116; dS. Xu, R. Chen, C. Zheng, W. Huang, *Adv. Mater.* **2016**, *28*, 9920-9940.

[2] a) H. Bhatia, I. Bhattacharjee, D. Ray, *J. Phys. Chem. Lett.* **2018**, *9*, 3808-3813; b) X. Ma, C. Xu, J. Wang, H. Tian, *Angew. Chem., Int. Ed.* **2018**, *57*, 10854−10858; c) L. Xu, G. Li, T. Xu, W. Zhang, S. Zhang, S. Yin, Z. An, G. He, *Chem. Commun.* **2018**, *54*, 9226−9229; d) L. Gu, H. Shi, C. Miao, Q. Wu, Z. Cheng, S. Cai, M. Gu, C. Ma, W. Yao, Y. Gao, Z. An, W. Huang, *J. Mater. Chem. C* **2018**, *6*, 226−233; e) Q. Wu, H. Ma, K. Ling, N. Gan, Z. Cheng, L. Gu, S. Cai, Z. An, H. Shi, W. Huang, *ACS Appl. Mater. Interfaces* **2018**, *10*, 33730−33736; f) Z. C. Cheng, H. F. Shi, H. L. Ma, L. F. Bian, Q. Wu, L. Gu, S. Z. Cai, X. Wang, W. W. Xiong, Z. F. An, W. Huang, *Angew. Chem., Int. Ed.* **2018**, *57*, 678−682; g) S. M. A. Fateminia, Z. Mao, S. Xu, Z. Yang, Z. Chi, B. Liu, *Angew. Chem., Int. Ed.* **2017**, *56*, 12160−12164; h) Z. Chai, C. Wang, J. Wang, F. Liu, Y. Xie, Y. Z. Zhang, J. R. Li, Q. Li, Z. Li, *Chem. Sci.* **2017**, *8*, 8336−8344..[3] a) Z. An, C. Zheng, Y. Tao, R. Chen, H. Shi, T. Chen, Z. Wang, H. Li, R. Deng, X. Liu, W. Huang, *Nat. Mater.* **2015**, *14*, 685-690; b) S. Cai, H. Shi, J. Li, L. Gu, Y. Ni, Z. Cheng, S. Wang, W.-w. Xiong, L. Li, Z. An, W. Huang, *Adv. Mater.* **2017**, *29*, 1701244; c) Y. Gong, G. Chen, Q. Peng, W. Z. Yuan, Y. Xie, S. Li, Y. Zhang, B. Z. Tang, *Adv. Mater.* **2015**, *27*, 6195-6201; d) J. Yang, X. Zhen, B. Wang, X. Gao, Z. Ren, J. Wang, Y. Xie, J. Li, Q. Peng, K. Pu, Z. Li, *Nat. Commun.* **2018**, *9*, 840; e) Z. Yang, Z. Mao, X. Zhang, D. Ou, Y. Mu, Y. Zhang, C. Zhao, S. Liu, Z. Chi, J. Xu, Y.-C. Wu, P.-Y. Lu, A. Lien, M. R. Bryce, *Angew. Chem. Int. Ed.* **2016**, *55*, 2181-2185; f) W. Zhao, Z. He, Jacky W. Y. Lam, Q. Peng, H. Ma, Z. Shuai, G. Bai, J. Hao, Ben Z. Tang, *Chem* **2016**, *1*, 592-602.

[4] a) S. Sarkar, H. P. Hendrickson, D. Lee, F. DeVine, J. Jung, E. Geva, J. Kim, B. D. Dunietz, *J. Phys. Chem. C* **2017**, *121*, 3771-3777; b) W. Z. Yuan, X. Y. Shen, H. Zhao, J. W. Y. Lam, L. Tang, P. Lu, C. Wang, Y. Liu, Z. Wang, Q. Zheng, J. Z. Sun, Y. Ma, B. Z. Tang, *J. Phys. Chem. C* **2010**, *114*, 6090-6099; c) S. Pan, Z. Chen, X. Zheng, D. Wu, G. Chen, J. Xu, H. Feng, Z. Qian, *J. Phys. Chem. Lett.* **2018**, *9*, 3939-3945.

[5] a) O. Bolton, K. Lee, H.-J. Kim, K. Y. Lin, J. Kim, *Nat. Chem.* **2011**, *3*, 205-210; b) S. K. Maity, S. Bera, A. Paikar, A. Pramanik, D. Haldar, *Chem. Commun.* **2013**, *49*, 9051-9053; c) H. Shi, Z. An, P.-Z. Li, J. Yin, G. Xing, T. He, H. Chen, J. Wang, H. Sun, W. Huang, Y. Zhao, *Cryst. Growth Des.* **2016**, *16*, 808-813; d) X. Sun, B. Zhang, X. Li, C. O. Trindle, G. Zhang, *J. Phys. Chem. A* **2016**, *120*, 5791–5797.

[6] a) O. Bolton, D. Lee, J. Jung, J. Kim, *Chem. Mater.* **2014**, *26*, 6644-6649; b) C. Li, X. Tang, L. Zhang, C. Li, Z. Liu, Z. Bo, Y. Q. Dong, Y.-H. Tian, Y. Dong, B. Z. Tang, *Adv. Opt. Mater.* **2015**, *3*, 1184-1190; c) X. Pang, W. J. Jin, in *Halogen Bonding II. Topics in Current Chemistry, Vol. 359* (Eds.: P. Metrangolo, G. Resnati), Springer International Publishing, Cham, **2015**, pp. 115-146; d) X. Pang, H. Wang, W. Wang, W. J. Jin, *Cryst. Growth Des.* **2015**, *15*, 4938-4945; e) S. d'Agostino, F. Spinelli, P. Taddei, B. Ventura, F. Grepioni, *Cryst. Growth Design* **2018**, DOI: 10.1021/acs.cgd.8b01443; f) L. Li, Z. F. Liu, W. X. Wu, W. J. Jin, *ActaCryst.* **2018**, *B74*, 610–617.

[7] a) E. Lucenti, A. Forni, C. Botta, L. Carlucci, A. Colombo, C. Giannini, D. Marinotto, A. Previtali, S. Righetto, E. Cariati, *ChemPhotoChem* **2018**, *2*, 801−805; b) E. Lucenti, A. Forni, C. Botta, L. Carlucci, C. Giannini, D. Marinotto, A. Pavanello, A. Previtali, S. Righetto, E. Cariati, *Angew. Chem. Int. Ed.* **2017**, *56*, 16302-16307.

[8] E. Lucenti, A. Forni, C. Botta, L. Carlucci, C. Giannini, D. Marinotto, A. Previtali, S. Righetto, E. Cariati, *J. Phys. Chem. Lett.* **2017**, *8*, 1894-1898.

10.1002/chem.201804980

WILEY-VCH

Entry for the Table of Contents
COMMUNICATION

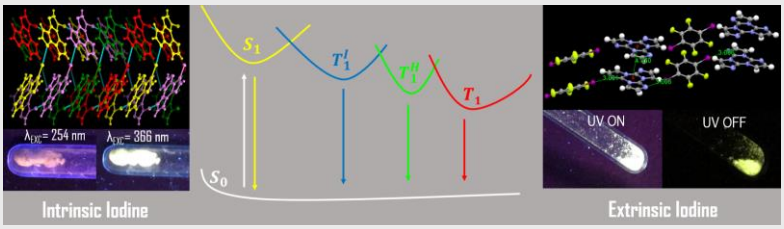

Elena Lucenti, Alessandra Forni, Chiara Botta,* Clelia Giannini, Daniele Malpicci, Daniele Marinotto, Andrea Previtali, Stefania Righetto and Elena Cariati**

Page No. – Page No.

Intrinsic and Extrinsic Heavy Atom Effect on the Multifaceted Emissive Behavior of Cyclic Triimidazole

Heavy halogen atoms can tune the emissive properties of organic luminogens both extrinsically and intrinsically. Here the two effects are investigated by comparing cyclic triimidazole (**TT**) with its mono-iodo derivative (**TTI**) and its cocrystal with diiodotetrafluorobenzene (**TTCo**). **TTI** shows a unique XB supported quadruple helix motif in its crystal structure.